https://doi.org/10.5194/egusphere-2026-3440
Preprint. Discussion started: 13 July 2026
© Author(s) 2026. CC BY 4.0 License.

Land-use-specific soil NO_x emissions in eastern China derived from TROPOMI observations

Yaqiu Zhao[1,2], Ronald J. van der A[3,4], Jieying Ding[3,4], Xiaojuan Lin[5,6], Qianqian Zhang[2]

[1]Chinese Academy of Meteorological Sciences, China Meteorology Administration, Beijing 100081, China
[2]National Satellite Meteorological Center, Key Laboratory of Radiometric Calibration and Validation for Environmental Satellites, Innovation Center for Fengyun Meteorological Satellite (FYSIC), China Meteorology Administration, Beijing 100081, China
[3]Royal Netherlands Meteorological Institute (KNMI), De Bilt, the Netherlands
[4]KNMI-NUIST Center for Atmospheric Composition, Nanjing University of Information Science & Technology (NUIST), Nanjing, China
[5]Laboratoire des Sciences du Climat et de l'Environnement, LSCE/IPSL, CEA-CNRS-UVSQ, Université Paris-Saclay, Gif-sur-Yvette, France
[6] Centre national d'études spatiales (CNES), 2 Place Maurice Quentin, 75039, Paris, France

Correspondence to: Qianqian Zhang (zhangqq@cma.gov.cn) and Jieying Ding (jieying.ding@knmi.nl)

Abstract.

Quantifying soil nitrogen oxide (NO_x) emissions is essential for constraining the nitrogen cycle and understanding its impacts on atmospheric chemistry and regional air quality. This study presents the first land-use-specific estimate of soil NO_x emissions across eastern China derived from TROPOMI satellite observations at a spatial resolution of 0.2º × 0.2º, covering forest, cropland, grassland/shrubland and bare land. We derive the emission intensity factor β for these land use types as functions of soil temperature (T_s) and soil volumetric water content (θ_v). Total soil NO_x emissions from eastern China in 2019 are estimated to be 1305 ± 368 Gg N, with largest contributions from cropland (623 ± 267 Gg N, ~ 48 %) and forest (486 ± 124 Gg N, ~ 37 %). High-emission areas (> 4 kg N ha^{-1} yr^{-1}) are concentrated in the North China Plain, and all land use types show summer-peak seasonal patterns. Soil NO_x emissions exhibit land-use-specific responses to temperature and moisture. Most land use types show a clear optimum temperature and high-temperature inhibition effect, which are captured by a Gaussian response function. We find that existing global emission inventories may underestimate soil NO_x emissions from forests in China. The comparison with other emission inventories and soil emission observations demonstrates that the proposed method provides a reliable basis for estimating soil NO_x emissions by capturing land-use-specific responses to environmental drivers. This satellite-based approach can provide input to the formulation of emission reduction strategies and support ecosystem management under climate change.

1 Introduction

Nitrogen oxides ($NO_x = NO + NO_2$) are critical air pollutants that pose significant threats to both human health and ecological environments. Long-term exposure to nitrogen dioxide (NO_2) is directly associated with premature mortality from cardiovascular and respiratory diseases (Depayras et al., 2018). Furthermore, NO_x participates in atmospheric photochemical

https://doi.org/10.5194/egusphere-2026-3440
Preprint. Discussion started: 13 July 2026
© Author(s) 2026. CC BY 4.0 License.

reactions, leading to the formation of ozone (O_3), a potent greenhouse gas that also causes substantial crop yield reductions (Steinkamp and Lawrence, 2009; Fowler et al., 2013; Zhang et al., 2021). Atmospheric oxidation of NO_x generates nitrate aerosol, contributing to both acid deposition and the formation of secondary fine particulate matter ($PM_{2.5}$) (Fowler et al., 2013), thereby further exacerbating air quality degradation and increasing health risks (Li et al., 2023a; Caplin et al., 2019; Zheng et al., 2019).

NO_x originates from fossil fuel combustion, biomass burning, lightning, and soil-atmosphere exchange processes (Denman, 2007; Schumann and Huntrieser, 2007; Logan, 1983). Among these, soil NO_x emissions represent the second largest contributor following combustion sources, accounting for approximately 15 % of the global total NO_x emissions (Weng et al., 2020; Holland, 1999; Vinken et al., 2014). In recent decades, stringent emission controls on combustion sources such as transportation, power plants, and industry have achieved notable success, leading to significant reductions in anthropogenic NO_x emissions across many regions (Zhang et al., 2003; Rafaj et al., 2013; Van Der A et al., 2017; Li et al., 2024a). Thus, the relative contribution of natural sources, particularly soil NO_x emissions, has gained increasing attention. Accumulating evidence indicates that soil NO_x emissions not only can cause substantial increase in surface O_3 concentrations (Sha et al., 2021; Wang et al., 2022) but can also offset the benefits achieved by anthropogenic emission controls (Lu et al., 2021; Guo et al., 2020; Wang et al., 2024). Given the backdrop of global warming and the increasing frequency of extreme climate events, the uncertainties associated with soil NO_x emissions are further amplified. Consequently, accurately quantifying soil NO_x emissions and identifying their spatiotemporal characteristics have emerged as critical challenges for current air quality and climate models.

The most widely used methods for estimating soil NO_x emissions include empirical statistical models, process-based models, and inversion methods using satellite observations. Process-based models, grounded in the conceptual "hole-in-the-pipe" framework (Firestone and Davidson, 1989), simulate the spatiotemporal dynamics of soil NO_x emissions at a mechanistic level. This method describes microbial processes such as nitrification and denitrification, along with their environmental regulators (e.g., moisture, temperature, soil properties) through mathematical equations. However, their capacity to accurately estimate emissions at regional scales is often constrained by uncertainties in the key mechanisms and the lack of required input soil parameters (e.g., soil pH, soil organic carbon) (Kesik, 2005; Butterbach-Bahl et al., 2009; Molina-Herrera et al., 2017). Empirical statistical models typically establish relationships between observed emission fluxes and key environmental or management factors (e.g., temperature, moisture, and nitrogen input) through statistical regression, which are then extrapolated to global scales (Yienger and Levy, 1995; Yan et al., 2005). The Yienger and Levy (1995) (YL95) scheme is still widely used in atmospheric chemistry models. Subsequent updates have improved emission factors for specific ecosystem types (Steinkamp and Lawrence, 2011) and introduced continuous physical response functions, such as the Berkeley-Dalhousie Soil NO_x Parameterization (BDSNP) (Hudman et al., 2012). These models employ simplified exponential functions or artificially set plateaus at high temperatures (e.g., > 30 °C) (Hudman et al., 2012; Weng et al., 2020). However, new evidence suggests that soil NO_x continue to rise significantly in certain regions within the 30–40 °C range (Wang et al., 2021). Therefore, despite

https://doi.org/10.5194/egusphere-2026-3440
Preprint. Discussion started: 13 July 2026
© Author(s) 2026. CC BY 4.0 License.

the increasing complexity of these empirical statistical models, they still suffer from a lack of detailed parameterization and limited universality of their response functions.

The increasing availability of satellite observation data has accelerated the development of top-down methods for deriving soil NO_x emissions. These approaches typically use satellite-observed NO_2 column concentrations from e.g. the Ozone Monitoring Instrument (OMI) or the Global Ozone Monitoring Experiment (GOME) instrument to adjust a priori emissions (including anthropogenic, soil, and lightning sources) within chemical transport models (CTMs) (e.g. GEOS-Chem). Soil NO_x emissions are subsequently separated from the total posterior emissions using attribution techniques. Early studies attributed the increments in total emissions to soil sources by identifying regions dominated by combustion or soil emissions based on prior information (Jaegle et al., 2005; Wang et al., 2007; Zhao and Wang, 2009). Recent studies have gradually improved soil NO_x attribution by incorporating statistical regression, mass balance, and nonlinear chemical corrections, making the separation more objective, reproducible, and applicable at global or high-resolution scales (Vinken et al., 2014; Lin, 2012). Despite these advances in soil NO_x attribution, two key limitations still exist. First, posterior soil NO_x estimates lack interpretability with respect to environmental drivers, as the response functions are prescribed in the prior emission model rather than dynamically constrained by the inversion. Second, although the satellite signal enables the estimation of soil NO_x emissions, the various sources of soil NO_x cannot be directly separated. While top-down estimates consistently suggest that bottom-up inventories underestimate soil NO_x emissions, substantial uncertainties in the quantifications remain (Vinken et al., 2014). Consequently, developing more robust and interpretable inversion frameworks for soil NO_x emissions based on satellite observation data remains a crucial research focus.

Here, we present a satellite-based gridded attribution approach to quantify soil NO_x across eastern China, a region characterized by intensive human activity and complex land use. By integrating top-down total emissions derived from the DECSO (Daily Emissions Constrained by Satellite Observations) algorithm (Mijling and Van Der A, 2012; Ding et al., 2017a; Van Der A et al., 2024) combined with other geophysical data, we separate soil NO_x through a multiple linear regression method. Our approach employs dynamic meteorological classifications based on soil temperature and soil volumetric water content to preserve spatial information and capture the effects of environmental variables. Furthermore, we introduce a Gaussian function in soil NO_x emission modelling to identify optimum emission temperatures and high-temperature inhibition effects. By applying this approach to eastern China for the year 2019, we aim to (1) develop a soil NO_x emission inventory derived from TROPOMI observations with robust uncertainty estimates, (2) characterize the land-use-specific responses of soil NO_x emissions to temperature and moisture, and (3) clarify the spatiotemporal patterns of land-use-specific emissions.

2 Data

2.1 Total satellite-derived NO_x emissions data

The total NO_x emissions data used in this study are derived from satellite NO_2 observations using the DECSO (Daily Emissions Constrained by Satellite Observations) algorithm (Mijling and Van Der A, 2012; Ding et al., 2017a; Van Der A et al., 2024).

https://doi.org/10.5194/egusphere-2026-3440
Preprint. Discussion started: 13 July 2026
© Author(s) 2026. CC BY 4.0 License.

This algorithm, based on an extended Kalman filter framework, optimizes the emissions by combining the simulation results of the chemical transport model (CHIMERE) (Menut et al., 2021) with satellite-observed tropospheric NO_2 column concentrations from the TROPOspheric Monitoring Instrument (TROPOMI) on the Sentinel-5 Precursor (S-5P) satellite (Veefkind et al., 2012). The original observations undergo quality control and are aggregated into "super-observations" matched to the model grid to improve data quality and reduce representativeness errors (Ding et al., 2020; Van Der A et al., 2024) using the method of Rijsdijk et al. (2025). NO_x emissions estimated by the DECSO algorithm represent total surface emissions from anthropogenic and natural sources, while contributions from lightning and the free troposphere are excluded, as the observations and their inversion are focused on the lower troposphere (below 500 hPa) (Van Der A et al., 2024). The DECSO algorithm has been validated and applied in multiple regional studies, including East Asia (Ding et al., 2020; Ding et al., 2017b; Ding et al., 2015), India (Ding et al., 2022), Europe (Van Der A et al., 2024), and the ocean region (Ding et al., 2018), demonstrating its robust ability to capture emissions from both anthropogenic and natural sources. Considering observational errors, model physics errors, and characterization errors, the uncertainty in monthly emissions estimates at the grid scale is approximately 25 % (Van Der A et al., 2024). This study uses monthly DECSO NO_x emission data for eastern China (102º–132º E, 18º–50º N) in 2019, with a spatial resolution of 0.2º × 0.2º. This region covers the major areas of human population in China.

2.2 Anthropogenic NO_x emissions data

This study uses the Air Benefit and Cost and Attainment Assessment System Emission Inventory (ABaCAS-EI) (Zhao et al., 2013; Zhao et al., 2018; Zheng et al., 2019) for the year 2019 as the anthropogenic emission data in the study area. The ABaCAS-EI inventory is developed based on activity-level data (such as energy consumption, industrial output, etc.) and emission intensity factors, with an overall uncertainty of approximately 35 % in its emission estimates (Li et al., 2024b; Zhao et al., 2013). Due to its long time series data, timely updates, and inclusion of more detailed emission source sectors, it is widely used in air pollutant studies in China (Li et al., 2023b; Zheng et al., 2019). Anthropogenic emission data for Taiwan is supplemented using the global monthly bottom-up anthropogenic NO_x emission inventory (CAMS-GLOB-ANT version 6.2) in 2019 since this region is not covered by the ABaCAS-EI. CAMS-GLOB-ANT is obtained from the Copernicus Atmospheric Monitoring Center, with a horizontal resolution of 0.1º × 0.1º (Soulie et al., 2024). The final anthropogenic NO_x emissions data are re-gridded to the spatial resolution of 0.2º × 0.2º of DECSO.

2.3 Soil temperature and soil moisture data

Soil temperature and soil moisture are factors that influence NO_x emissions by affecting microbial activity. We use the soil temperature (T_s) and soil volumetric water content (θ_v) data from the land component (ERA5-Land) of the fifth generation of the European ReAnalysis dataset (ERA5) of the European Centre for Medium-Range Weather Forecasts (ECMWF) (Muñoz-Sabater et al., 2021) to address their influence on soil NO_x emissions. This dataset provides long-term, consistent, and high-quality estimates of global land surface variables by assimilating ERA5 data with global observation system data and running

https://doi.org/10.5194/egusphere-2026-3440
Preprint. Discussion started: 13 July 2026
© Author(s) 2026. CC BY 4.0 License.

it in the high-resolution land surface model: the Carbon Hydrology-Tiled ECMWF Scheme for Surface Exchanges over Land (CHTESSEL) (Zheng et al., 2024). We extract monthly mean surface soil (0–7 cm depth) temperature and volumetric water content data from 2019 with an original spatial resolution of 0.1º × 0.1º and re-grid them to 0.2º × 0.2º.

2.4 Land use/Land cover (LULC) data

In addition to soil temperature and moisture, studies have also shown that soil NO_x emissions vary significantly among different vegetation types (Verchot et al., 1999; Vinken et al., 2014; Yan et al., 2005). The land use/land cover dataset used in this study is the 100-meter spatial resolution dynamic global land cover product (CGLS-LC100m) for 2019 (version 3.0.1; Buchhorn et al., 2020a, 2020b) published by the Copernicus Global Land Service (CGLS). The product is based on PROBA-V satellite time-series imagery and uses the United Nations Land Cover Classification System (UN-LCCS) to provide land use classification information. We regrouped the initial 22 land use types in the LULC database into the following 7 main types: marine, urban, cropland, bare land, inland water, forest, and grassland/shrubland. Four land use/land cover types are focused on in this study to estimate soil NO_x emissions: forest, cropland, grassland/shrubland, and bare land. The original 100-meter resolution LULC product is re-gridded to the 0.2° DECSO grid. In each 0.2° grid cell, the fraction of each land use type is defined as the land use ratio (LUR), which will be used for subsequent grid cells selection and fitting parameters.

3 Method

The method used in this study is an improvement upon the method developed by Lin et al. (2024) for separating soil emissions from total NO_x emission data retrieved from satellite observations. Lin et al. (2024) identified grid cells dominated by targeted land use types for different climate zones. Then, the soil NO_x emissions are assigned to different biogenic sources through a series of multiple linear functions. By solving these functions, an "emission intensity factor" β is defined as the emission intensity of a certain land use type when LUR=1 is obtained. Compared to Lin et al. (2024), we improve the method in two aspects. First, the meteorological influences on soil NO_x emission are considered by introducing the T_s and θ_v into the function instead of using climate zone categories. By replacing the calculation of averages within coarse climatic zones with meteorological classification and regression calculations based on grid cells, we addressed the spatial discontinuities and abrupt changes in zonal boundaries present in the results of Lin et al. (2024). Second, we use a multiple linear regression model for each grid cell instead of the regional average matrix calculation to preserve spatial information and facilitate the exploration of its relationship with meteorological factors. This method is developed for eastern China, but it can be easily applied to other regions. A flowchart of the improved method is provided in Fig. 1.

https://doi.org/10.5194/egusphere-2026-3440
Preprint. Discussion started: 13 July 2026
© Author(s) 2026. CC BY 4.0 License.

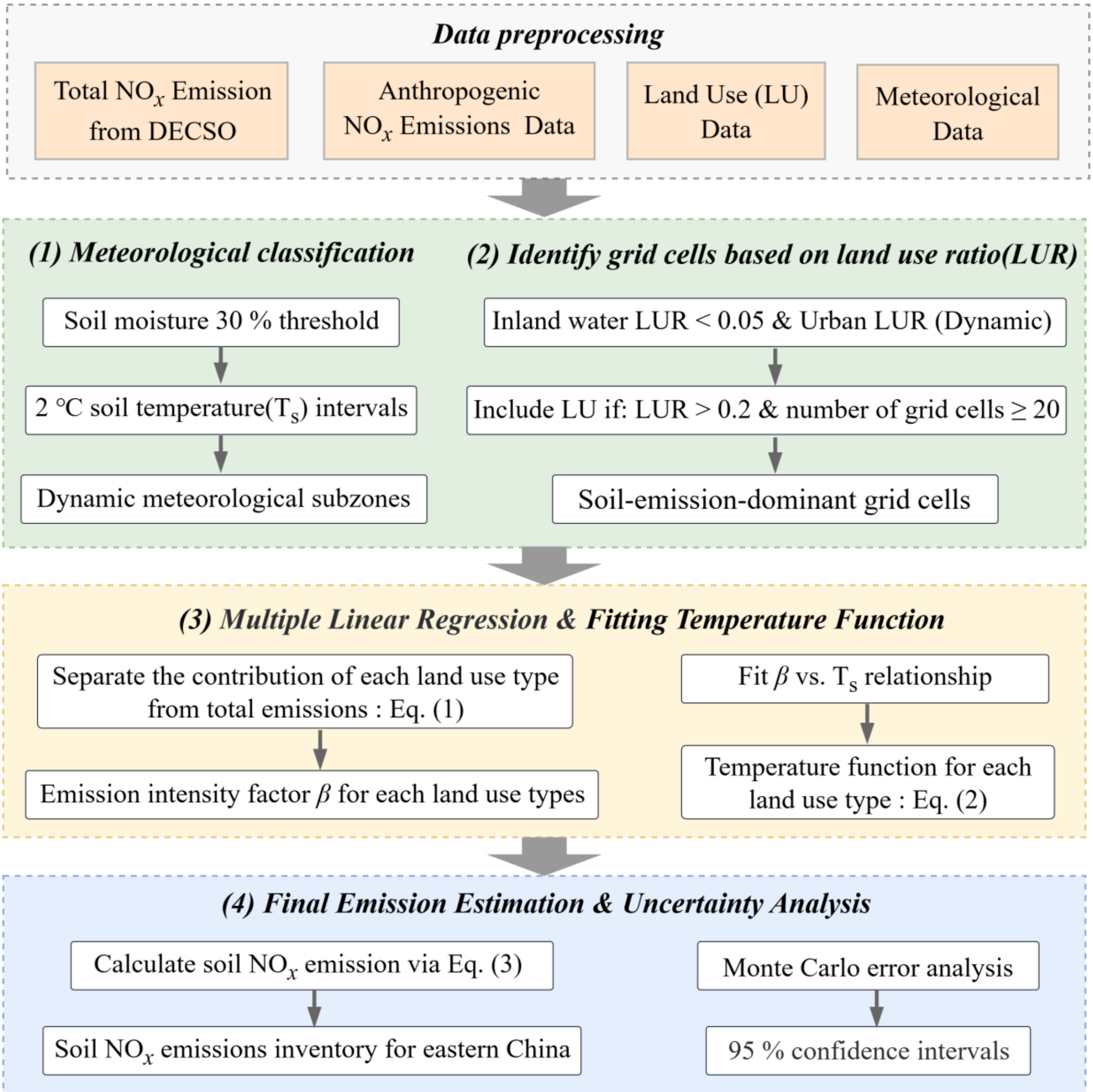

Figure 1: Flowchart for soil NO_x emission estimation of the improved method.

3.1 Meteorological classification

160 Meteorological factors are the main drivers of nitrification and denitrification, which produce soil NO_x (Firestone and Davidson, 1989). Soil moisture controls oxygen transport and gas diffusion, and soil temperature regulates microbial enzymatic reactions and mineralization rates (Pilegaard, 2013). Compared to using the Köppen-Geiger climate classification (Lin et al., 2024;

https://doi.org/10.5194/egusphere-2026-3440
Preprint. Discussion started: 13 July 2026
© Author(s) 2026. CC BY 4.0 License.

Kottek et al., 2006), dividing the study domain based on T_s and θ_v can more directly characterize the impact of meteorology on soil NO_x emissions and avoids the spatial discontinuity of pre-set climate boundaries.

We define the grid cells with θ_v equal to or lower than 30 % as the dry zone and those above 30 % as the wet zone, to ensure that both zones contain sufficient grid cells to calculate β for main land use types. Then, within each zone, subzones are divided at 2 °C monthly mean T_s intervals for the same reason. Since the classification is based on monthly mean T_s and θ_v, the subzones vary dynamically month by month, which can better reflect the changes in meteorological conditions throughout the year. For each dynamic subzone, we apply the multiple linear regression model which will be described in Sect. 3.3 to the grid cells identified as soil-emission-dominant (Sect. 3.2). This regression yields a set of emission intensity factors β (one for each land use type). Subsequently, for each land use type and separately for the dry and wet zones, we use β values obtained from all temperature subzones to explore the relationship between emission intensity factor β and T_s (Eq. 2).

3.2 Soil-emission-dominant grid cells identification

Before applying the regression model within each subzone, we first identify soil-emission-dominant grid cells based on land cover products, as described below. To ensure the accuracy of the regression, we exclude grid cells significantly affected by non-soil factors, including inland water bodies and urban areas. For inland water bodies, any grid cell with an inland water LUR greater than 0.05 is excluded. This threshold is set to conservatively remove grid cells where water coverage is substantial, thereby minimizing the potential interference from ship-borne NO_x emissions (Zhang et al., 2023). For urban areas we use dynamic thresholds, since the ratio of anthropogenic to natural emissions varies seasonally. In cold seasons (October to March), emissions are mainly from anthropogenic sources, thus strict limits are required: a grid cell in cold seasons is retained only if its urban LUR is less than 0.01 and its annual mean DECSO NO_x emissions are less than or equal to 7.5 kg N ha^{-1} yr^{-1}. The strict LUR limit (0.01) filters out mixed urban-rural grid cells, while an upper limit of the emission threshold (7.5 kg N ha^{-1} yr^{-1}) derived from observed emissions in low-emission urban areas in eastern China ensures selected cells represent near-background levels. In warm seasons (April to September) with increased biological activity, a grid cell is retained only if its urban LUR is less than 0.02. The seasonal varying thresholds allow more grid cells with higher natural contribution to be included while still exclude dense urban areas.

3.3 The multiple linear regression model

Before performing multiple linear regression, we need to exclude remaining anthropogenic emissions in selected grid cells, which are subtracted from the total DECSO NO_x emissions. Note that this is only performed on the grid cells identified as soil-emission-dominant, where anthropogenic emissions are minor. If a grid cell results in a negative value after subtraction, it is set to be zero. This operation is only for preliminary noise reduction, while the subsequent multiple linear regression can distinguish the emission contributions of different land use types and establish a functional relationship between emissions and meteorological factors.

https://doi.org/10.5194/egusphere-2026-3440
Preprint. Discussion started: 13 July 2026
© Author(s) 2026. CC BY 4.0 License.

Using the selected soil-emission-dominant grid cells, we build a multiple linear regression algorithm to establish a relationship between the land use types and the soil NO_x emissions. The algorithm is built for all subzones in each month, presented as Eq. (1):

$$E_p(i)=\beta_{forest}\cdot R_{forest}(i)+\beta_{crop}\cdot R_{crop}(i)+\beta_{shrub}\cdot R_{shrub}(i)+\beta_{bare}\cdot R_{bare}(i) \quad (1)$$

Here, $E_p(i)$ represents the preliminary estimate of total soil NO_x emission value for grid cell i with the unit kg N ha^{-1} yr^{-1}, calculated as the DECSO emissions corrected by subtracting anthropogenic emissions for soil-emission-dominant grid cells. $R(i)$ denotes the land use ratio of a certain land type in each grid cell (i.e., LUR is defined in Sect. 2.4.). β is the emission intensity factor, in kg N ha^{-1} yr^{-1}. Solving Eq. (1) through least squares regression within each dynamic subzone yields a set of β values. These β values are key intermediate output parameters of this method. They quantify the estimated emission intensity contributed by a single (LUR=1) land use type under specific T_s and θ_v conditions within that subzone. Essentially, the algorithm separates the emission contribution of each land use type from the mixed total emissions. Furthermore, β is used to subsequently explore the relationship between emissions and T_s for each land use type under dry or wet conditions (based on θ_v). If there are fewer than 20 grid cells with a LUR > 0.2 for a certain land use type, we consider that land use type not to be a major emission source. To ensure the stability of the regression model and the representativeness of the results, that land use type is removed from the equation for a subzone.

3.4 Functional fitting of emission intensity factors and final emission estimation

Since we define the subzones on a narrow temperature interval of 2 ℃, we collect β values from each dynamic subzones throughout the year, which are sufficient to analyse their variation with T_s. During the fitting process, we take the median β value from various month within each temperature interval as the representative value, and the β vs T_s relationship is fitted for every land use type in wet and dry soil moisture conditions separately. Two candidate functions are considered to characterize the β vs T_s relationship. One is a simple exponential function, commonly used in existing soil NO_x emission models (e.g. YL95, BDSNP models and MEGAN v2.04) (Hudman et al., 2012; Morichetti et al., 2022; Yienger and Levy, 1995). The other is a Gaussian model, introduced in this study to capture optimum temperature and high-temperature inhibition effect observed in experimental studies on microbial activity (Pietikainen et al., 2005; Pilegaard, 2013). β can be represented as a function of T_s:

$$\beta(T_s) = a\, e^{b\, T_s} \quad (2a)$$

$$\beta(T_s) = c\, exp\left[-\frac{(T_s-T_{s0})^2}{2\sigma^2}\right] + d \quad (2b)$$

Where T_s represents the soil temperature (℃), T_{s0} is the optimum temperature (℃). β is the emission intensity factor (kg N ha^{-1} yr^{-1}). The equation parameters (a, b, c, T_{s0}, σ, d) are fitted using the β values for each land use type under dry/wet conditions obtained in Sect. 3.3. The selection of the optimal model for each land use type and moisture condition is presented in Sect. 4.1.

https://doi.org/10.5194/egusphere-2026-3440
Preprint. Discussion started: 13 July 2026
© Author(s) 2026. CC BY 4.0 License.

In summary, Eq. (1) separates the discrete emission intensity factors (β) for each land use type within specific temperature and moisture intervals from the total soil NO_x emissions. These discrete values are then parameterized into continuous temperature response functions through Eq. (2). Consequently, we estimate the total soil NO_x emissions using the temperature function for each land use type under two moisture conditions as represented in:

$$E_s(i)=\beta_{forest}(T_s)\cdot R_{forest}(i)+\beta_{crop}(T_s)\cdot R_{crop}(i)+\beta_{shrub}(T_s)\cdot R_{shrub}(i)+\beta_{bare}(T_s)\cdot R_{bare}(i) \quad (3)$$

To ensure that the estimated soil emissions E_s do not exceed the total emissions constraint from satellite inversions, the DECSO value is used as the upper limit if the calculated value for a grid cell exceeds the DECSO emissions. Finally, the anthropogenic emissions for each grid cell are considered to be the difference between the total NO_x emissions data from DECSO for that grid cell and the estimated E_s.

3.5 Uncertainty assessment

We employ a Monte Carlo error analysis method to assess the uncertainty of soil NO_x emission estimates. It is a numerical method that quantifies the variability of model outputs through repeated random sampling (Metropolis and Ulam, 1949), and is widely used in studies to evaluate emission inventories (e.g. Del Grosso et al., 2010; Winiwarter and Muik, 2010; Frey et al., 1998; Sun et al., 2021; Wei et al., 2011; Cao et al., 2026).

In our study, the uncertainties of the estimated soil NO_x emissions mainly are associated with the input variables in the calculation process. The input variables include:

(a) The total and anthropogenic NO_x emissions. As we stated above, we use DECSO total NO_x emission data as the observed total NO_x emissions for soil-dominated grid cells, with an uncertainty of approximately 25 %. The anthropogenic ABaCAS emissions inventory has a 35 % uncertainty.

(b) The soil temperature data. As a vital variable that drives the β function, soil temperature from ERA5-Land reanalysis datasets contains observation and assimilation errors. Evaluation studies of ERA5-Land indicate that the root mean square error (RMSE) of soil temperature across different regions typically ranges from 2.6 ℃ to 11.2 ℃ (Tan et al., 2025; Yang et al., 2020; Cao et al., 2020). Given the corresponding range of temperature variations, the relative uncertainty of soil temperature is estimated between 12 % and over 30 %. Since large errors usually occur in high-latitude or high-altitude areas with complex terrain, and most of our study area is agricultural and low-altitude, this study adopts a 15 % uncertainty for the soil temperature data.

(c) The land use ratio. Land use/land cover data contain classification errors and the re-gridding process introduces systematic biases. Cropland has the highest uncertainty, influenced by land fragmentation and land use dynamics related to agricultural management. Stable land cover types such as forest and bare land generally demonstrate higher

https://doi.org/10.5194/egusphere-2026-3440
Preprint. Discussion started: 13 July 2026
© Author(s) 2026. CC BY 4.0 License.

classification reliability. Therefore, we set the LUR error at 30 % for cropland, 20 % for grassland/shrubland, and 15 % for forest and bare land.

In the Monte Carlo analysis, each error source is independently and randomly sampled within their uncertainty ranges to run the simulation for 1000 times. These simulations are used to derive the mean, standard deviation, and coefficient of variation of emissions for each land use type and total emissions. The 95 % confidence interval is determined using the percentile method (2.5th~97.5th).

4 Results and discussion

4.1 Response of emissions to soil temperature and moisture conditions

By fitting the relationship between β and T_s with two candidate functions, we obtain the best fitting function for each land use type under two soil moisture conditions. Figure 2 illustrates the variation of β with soil temperature and the nonlinear fitting results for forest, cropland, grassland/shrubland, and bare land under low ($\theta_v \leq 30$ %) and high ($\theta_v > 30$ %) moisture conditions. The Gaussian function provides the best fit for forest soils under both moisture conditions, capturing a clear unimodal β vs T_s relationship (Fig. 2a). Under wet conditions, the model shows a high correlation (R^2 = 0.89), with emissions generally increasing with temperature to a maximum at approximately 22.0 °C, after which a high-temperature inhibition effect leads to a decline of β. This high-temperature inhibition effect is consistent with a recent in situ warming experiment in a temperate forest, which shows that a 2 °C increase reduces soil NO_x emissions by 19 % due to warming-induced soil drying that limits microbial N transformation (Huang et al., 2025). Under dry conditions, a similar unimodal pattern is observed with the optimum temperature also around 23.0 °C. However, the relatively lower R^2 (0.58) under dry condition indicates that the low soil water content may weaken the dominant driving force of temperature on emissions.

Figure 2b shows that the cropland soil NO_x emissions behave differently under different soil moisture conditions. When cropland moisture is lower than 30 %, a Gaussian function provides the best fit (R^2 = 0.61), with emissions peaking around 32.0 °C, near the upper limit of our temperature range. This suggests that the high-temperature inhibition effect may occur beyond this temperature range. When θ_v is higher than 30 %, NO_x emissions from cropland soil show an exponential growth trend with T_s (R^2 = 0.46). The low correlation of soil NO_x emission and temperature under wet conditions can likely be explained by the influence of intensive anthropogenic activities (e.g., fertilization and irrigation) in well-irrigated croplands, which introduce additional variability not captured by temperature and moisture alone (Zhou et al., 2010). Under wet conditions, the absence of an observed optimum temperature may reflect the influence of intensive agricultural management. Continuous nitrogen input from fertilization prevents microbes from being substrate-limited at high temperatures, while irrigation maintains adequate soil moisture and avoids drought stress (Dai et al., 2020). This makes it difficult to reach the potential optimal temperature which may lie beyond our observed temperature range. Overall, the promoting effect of high temperature on NO_x emissions from cropland soil dominates across the observed temperature range.

https://doi.org/10.5194/egusphere-2026-3440
Preprint. Discussion started: 13 July 2026
© Author(s) 2026. CC BY 4.0 License.

For grassland/shrubland under wet conditions, the Gaussian function provides the best fit ($R^2 = 0.78$), with emissions peaking around 14.0 °C followed by the high-temperature inhibition effect (Fig. 2c). However, for moisture conditions with $\theta_v < 30\%$, an exponential function best describes the β vs T_s relationship ($R^2 = 0.76$), with emissions increasing monotonically across the observed temperature range. This likely reflects a sampling limitation rather than an emission mechanism difference. Dry-zone grassland/shrubland grid cells in our study domain are primarily located in temperate and semi-arid regions where monthly mean T_s rarely exceeds 20 °C, resulting in insufficient sampling of the high-temperature range. Given that unimodal responses are observed in other natural land use types (forest, bare land and grassland/shrubland in wet-zones), grassland/shrubland in dry-zones may also exhibit optimal T_s and high-temperature inhibition effects at temperatures beyond our observational range, as discussed above for cropland in this section. This uncertainty should be considered when applying the fitted function to future warmer climate scenarios. We also note two outliers for $\theta_v \leq 30$ % near −4 °C that form a potential local peak in the β vs T_s scatter of Fig. 2c. Since this temperature range corresponds to the cold months of November-February, we examine the spatial distribution of grassland/shrubland β across these four months (Fig. 3). The results show that β is notably higher in December and January than in November and February, despite the former having lower temperatures. Given that biogenic soil NO_x emissions are very low under such cold conditions, the most likely explanation is that anthropogenic NO_x from heating intensifies during the coldest months and is not fully captured by the anthropogenic emission inventory, leaving a residual signal that is attributed to soil emissions in our regression analysis. Nevertheless, this potential bias has little influence on our fitted function, as the exponential model selected for dry-zone grassland/shrubland is not sensitive to these two outliers.

Since bare land is predominantly distributed in low-moisture areas, the analysis of the β vs T_s relationship is restricted to the dry conditions (Fig. 2d). It exhibits a Gaussian trend with a gradual increase in temperature ($R^2 = 0.81$). Above 15 °C, the β growth rate begins to increase, and the peak emission is expected to occur around 32 °C. However, the β of bare land remains consistently below 4 kg N ha^{-1} yr^{-1}, indicating a lower emission potential compared to other land use types.

https://doi.org/10.5194/egusphere-2026-3440
Preprint. Discussion started: 13 July 2026
© Author(s) 2026. CC BY 4.0 License.

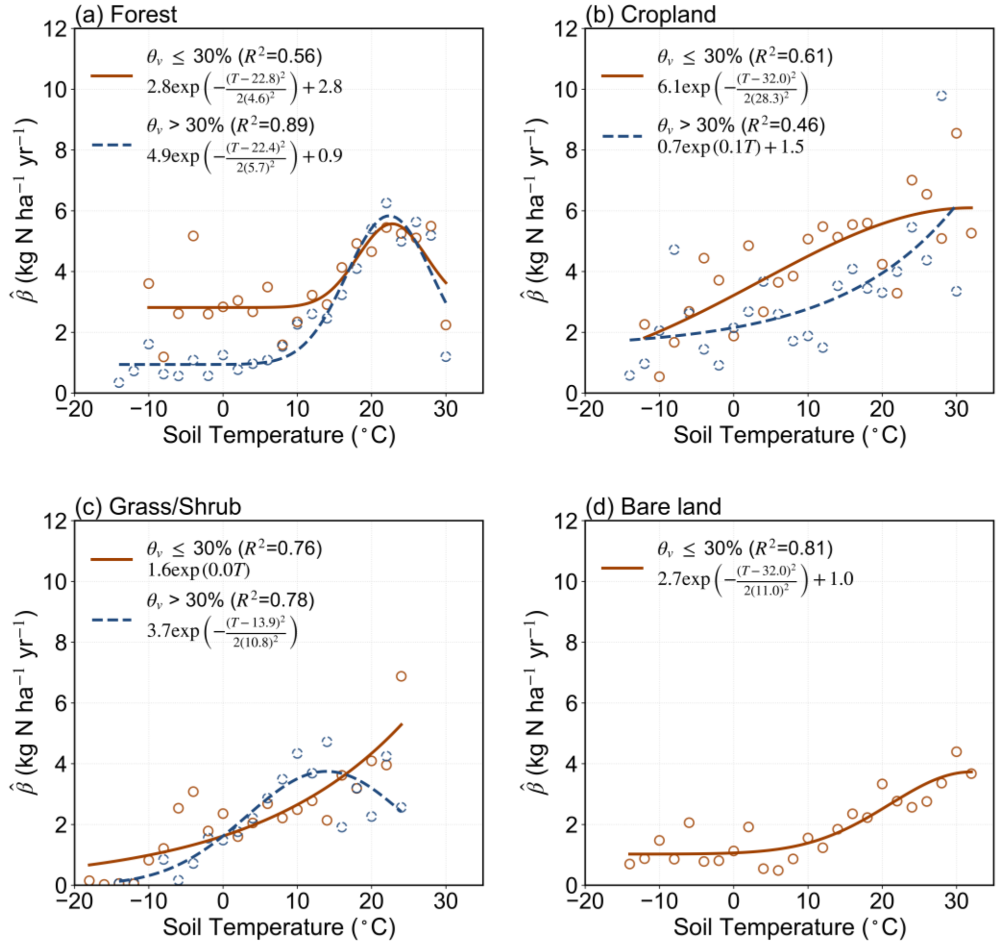

Figure 2: Response of emission intensity factor (β) to soil temperature (T_s) and soil moisture content (θ_v) for 4 land use types: forest (a), cropland (b), grass/shrub (c) and bare land (d). When θ_v > 30 %, there are not enough observations over bare land to derive the function. The results shown here are for 2019.

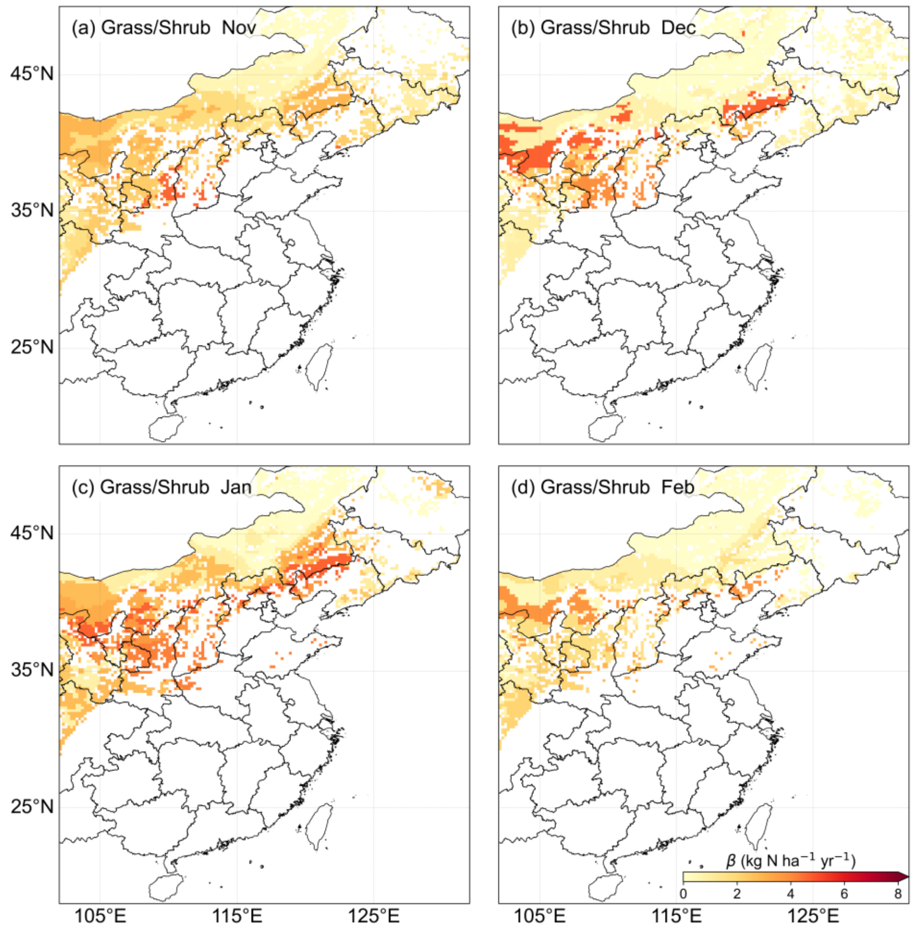

Figure 3: Spatial distribution of the grassland/shrubland emission intensity factor (β) for November (a), December (b), January (c), and February (d). Each colored pixel indicates a soil-emission-dominant grid cell selected in Sect. 3.2, with its color representing the β value derived from the temperature-moisture subzone to which that grid cell belongs in the multiple linear regression (Sect. 3.3). White areas within China indicate grid cells excluded from the regression.

4.2 Spatiotemporal patterns of the estimated emissions

Based on the β calculated for each land use type and Eq. 3, total soil NO_x emissions from eastern China in 2019 derived from satellite observation are 1305 ± 368 Gg N (mean ± std), representing approximately 20 % of the total NO_x emissions. This fraction falls within the reported range of 12 %–20 % for soil NO_x emissions at the global scale (Weng et al., 2020; Vinken et al., 2014; Yan et al., 2005) and is broadly consistent with regional estimates for China. For instance, soil NO_x emissions from fertilized cropland alone accounted for 17.3 % of total NO_x emissions in China in 2017 (Shen et al., 2022), while a combined study of field measurements and models estimated the contribution of terrestrial ecosystem NO_x emissions at approximately 18 % of anthropogenic emissions (Huang and Li, 2014). The slightly higher fraction derived in this study may reflect the context of declining anthropogenic NO_x emissions in recent years, as ambient NO_2 concentration has decreased by approximately 33 % across monitoring sites in China during 2015–2023 (Wang et al., 2024).

https://doi.org/10.5194/egusphere-2026-3440
Preprint. Discussion started: 13 July 2026
© Author(s) 2026. CC BY 4.0 License.

The estimated soil emissions exhibit significant spatial and seasonal variation (Fig. 4). High-emission areas with emission intensity exceeding 4 kg N ha^{-1} yr^{-1} are mainly concentrated in the North China Plain (e.g., Shandong, Henan, and Hebei provinces), the Yangtze River Delta, and parts of South China. These high-emission areas generally coincide with regions with intensive agricultural activity and favourable hydrothermal conditions. In contrast, soil emissions are relatively low (<1 kg N ha^{-1} yr^{-1}) in the western and northern border regions, which are generally sparsely vegetated or arid. Monthly soil NO_x emissions exhibit a clear seasonal variation, with a unimodal distribution peaking in summer. Winter (December to February) emissions are approximately 60–80 Gg N month^{-1}, while the highest emissions in July exceed 155 Gg N month^{-1}. The summer peak is likely driven by the combined effects of temperature-stimulated microbial activity across all land use types and fertilization during the crop growing season in agricultural regions.

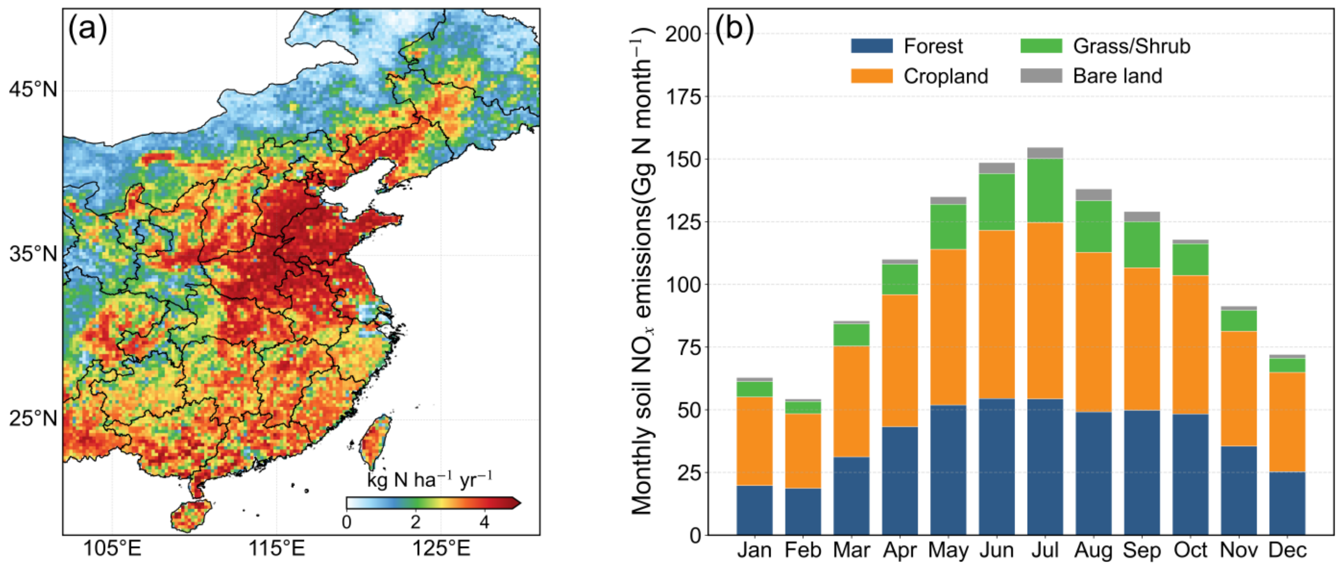

Figure 4: Spatiotemporal distribution of nitrogen oxide emissions from soil in China. (a) Spatial distribution averaged over 2019; (b) Monthly variation of emissions by component and total soil emissions in 2019.

Figure 5 illustrates the estimated soil NO_x emissions across four land use types. Forest emissions display distinct geographical patterns, with high emission areas predominantly located in the hilly and mountainous areas of southern and northeastern China. In southern subtropical forests (e.g., Guangdong, Guangxi, and Fujian), emissions are relatively high (2.0–3.5 kg N ha^{-1} yr^{-1}), and likely driven by the warm and humid climate. Cropland emissions are highly concentrated over the North China Plain, primarily attributed to high-density application of synthetic nitrogen fertilizers and double-cropping rotation. Significant cropland emissions are also observed in the Northeast Plain and the Sichuan Basin. In contrast, grassland/shrubland and bare land contribute significantly less to total soil NO_x emissions. Grassland/shrubland emissions are primarily distributed in semi-arid transition zones, such as the Loess Plateau and parts of Inner Mongolia, with intensities generally below 2.5 kg N ha^{-1} yr^{-1}. Bare land emissions are minimal and largely confined to the arid northwest.

https://doi.org/10.5194/egusphere-2026-3440
Preprint. Discussion started: 13 July 2026
© Author(s) 2026. CC BY 4.0 License.

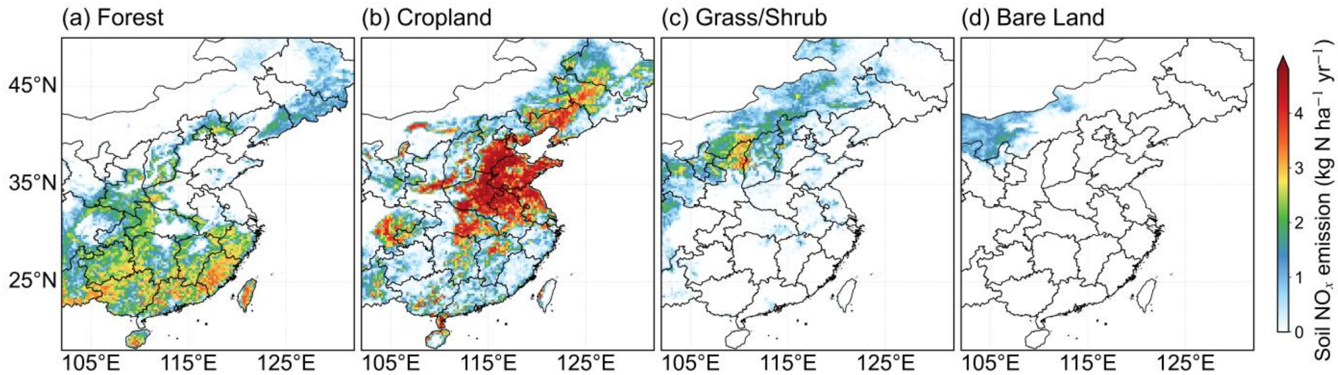

Figure 5: Spatial distribution of annual NO_x emissions from soil in 2019 in (a) forests, (b) croplands, (c) grassland/shrubland, and (d) bare lands.

As shown in Figs. 4b and 6, seasonal variations in emissions for each land use type are similar, but their emission magnitudes differ considerably. Forest emissions peak in summer, driven by warmer temperatures and monsoon precipitation that elevate emissions from both subtropical forests of southern China and temperate forests of northeastern China (Fig. 6). Notably, forest emissions remain relatively high into autumn (Fig. 4b), likely due to sustained favourable hydrothermal conditions in the extensive subtropical forests of southern China during this season. Cropland is the dominant source of soil NO_x emissions across all seasons, as illustrated by Fig. 4b. Although cropland emissions also peak in summer, they maintain high emission intensity through spring and autumn and remain the largest contributor even in winter (Fig. 6). This sustained contribution reflects the persistent influence of fertilization and irrigation in major agricultural regions such as the North China Plain (NCP) (Zhang et al., 2025). It should be noted that the meteorological factors-based method used in this study does not explicitly account for fertilization timing, and thus the influence of fertilizer application on the seasonal variability of cropland emissions may be underestimated. Incorporating more detailed cropland classification data and crop-specific fertilization calendars could further improve the accuracy of cropland emission estimates in future work. Grassland/shrubland emissions follow a similar seasonal pattern, peaking in summer when higher temperatures stimulate microbial activity, though their absolute contribution remains smaller. Bare land emissions are negligible throughout the year and originate primarily from the arid northwest. Therefore, the seasonal pattern of total soil NO_x emissions is shaped primarily by the year-round dominance of cropland emissions combined with the pronounced summer increase from forests and grassland/shrubland.

https://doi.org/10.5194/egusphere-2026-3440
Preprint. Discussion started: 13 July 2026
© Author(s) 2026. CC BY 4.0 License.

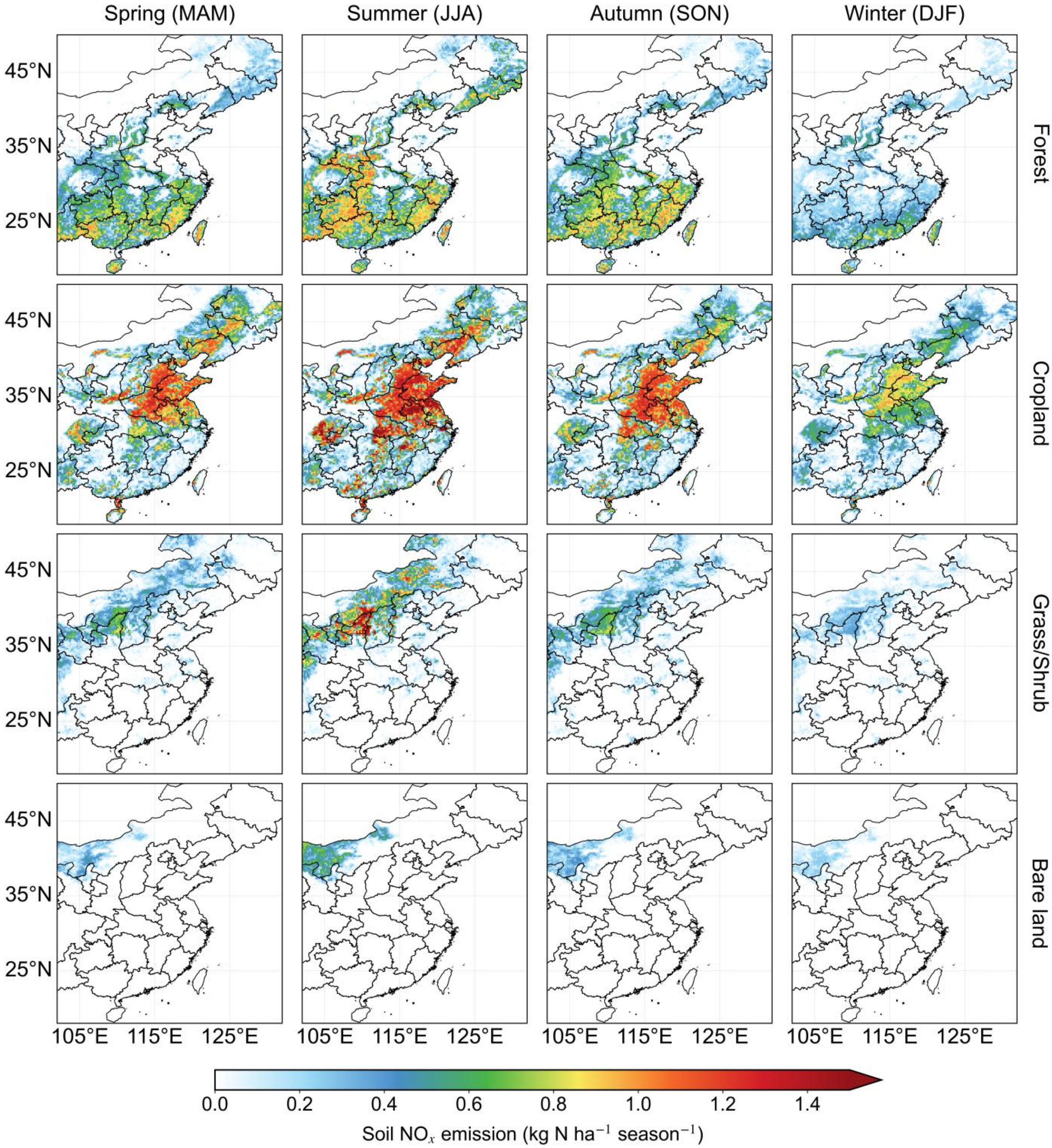

365 **Figure 6: Spatial distribution of soil NO$_x$ emissions in different seasons for different land use types in 2019.**

https://doi.org/10.5194/egusphere-2026-3440
Preprint. Discussion started: 13 July 2026
© Author(s) 2026. CC BY 4.0 License.

4.3 Comparison with existing emission inventories and studies

Table 1 details the estimated annual soil NO_x emissions from eastern China in 2019, the emission intensity, and the estimation uncertainties. Significant differences are found among different land use types, with cropland emerging as the primary contributor, followed by forests, grassland/shrubland, and bare land.

Table 1: Annual soil NO_x emissions and emission intensities for different land use type from eastern China in 2019.

Source	Emission (Gg N yr^{-1}) (mean ± std)	Intensity (kg N ha^{-1} yr^{-1})
Forest	486 ± 124	2.5
Cropland	623 ± 267	3.8
Grassland/Shrubland	165 ± 50	1.9
Bare Land	31 ± 7	1.1
Total	1305 ± 368	2.6

We compare the spatiotemporal variability of soil NO_x emissions from eastern China estimated in this study with two widely used global emission inventories. One is the CAMS soil emission inventory (CAMS-GLOB-SOIL version 2.4, called CAMS-soil), which provides global monthly soil NO_x emission grid data with a spatial resolution of 0.5º × 0.5º (Simpson et al., 2025; Simpson and Darras, 2021). The other is the Harvard-NASA Emissions Component (HEMCO) soil emission inventory (called HEMCO-soil), which provides global hourly soil NO_x emission data with a horizontal resolution of 0.25º latitude × 0.3125º longitude (Keller et al., 2014; Weng et al., 2020). As illustrated in Fig. 7a, all three inventories exhibit a consistent seasonal trend, with emissions peaking in summer (June-July) and declining to a minimum in winter. This consistency reflects the promoting effects of temperature and moisture on microbial activity, as well as the combined driving force of agricultural fertilization activities during the crop growing season on soil NO_x emissions. However, the monthly soil NO_x emissions estimated in this study are significantly higher than the other two inventories in 2019. The HEMCO-soil estimate is the lowest, especially approaching zero during November to February. While the CAMS-soil estimates are intermediate between HEMCO and our results, its peak summer values remain approximately 20 %–30 % lower than our result. Spatially, all three datasets identify the NCP as a dominant hotspot (Figs. 7b-d), driven by intensive agricultural management. Nevertheless, for non-cropland regions, HEMCO-soil and CAMS-soil generally show lower emission intensities, while this study reveals relatively high emission intensities in areas such as the Northeast forest region and the South China hilly forest region.

https://doi.org/10.5194/egusphere-2026-3440
Preprint. Discussion started: 13 July 2026
© Author(s) 2026. CC BY 4.0 License.

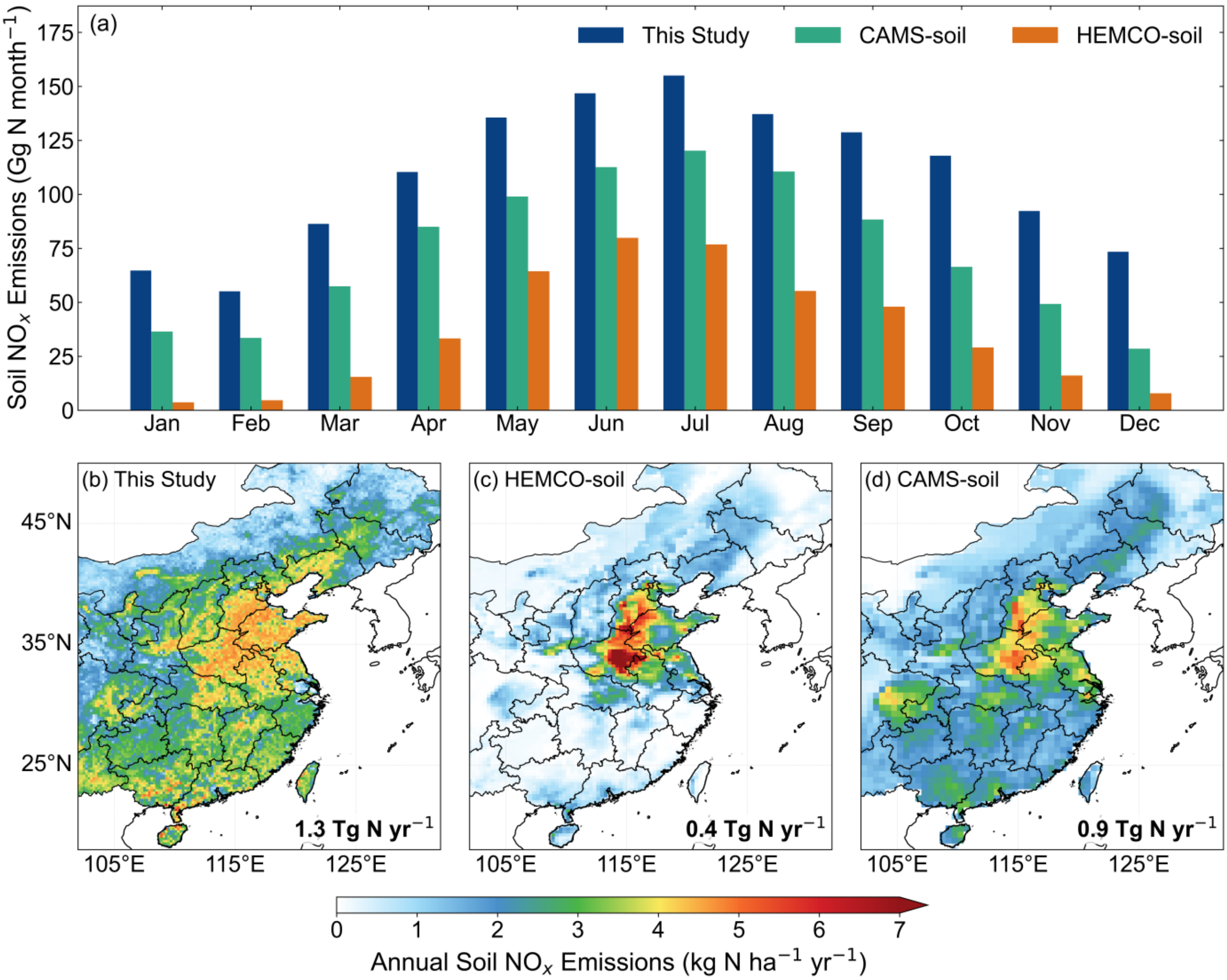

Figure 7: Comparison of soil NO$_x$ emission inventories. (a)Monthly comparison of soil NO$_x$ emissions from the three emission inventories. (b) Spatial distribution of soil NO$_x$ emissions estimated in this study, total soil NO$_x$ emissions from eastern China in 2019 are 1.3 Tg N. (c) Spatial distribution of the HEMCO-soil inventory, total soil NO$_x$ emissions from eastern China in 2019 are 0.4 Tg N. (d) Spatial distribution of the CAMS-soil inventory, total soil NO$_x$ emissions from eastern China in 2019 are 0.9 Tg N.

We further evaluate our estimates against those reported in previous studies (Fig. 8). Figure 8a shows that published estimates of total soil NO$_x$ emissions from China range widely from 380 to 1375 Gg N yr^{-1}, reflecting considerable uncertainty among empirical statistical models (Yan et al., 2005; Tie et al., 2006; Huang and Li, 2014), satellite-based top-down inversions (Lin, 2012; Wang et al., 2007), and mechanistic process-based simulations (Lu et al., 2021). Our estimated total soil NO$_x$ emissions for 2019 are at a relatively high level among all the estimations. Specifically, our results are significantly higher than those estimated using satellite-based methods and certain statistical model approaches. This difference may stem from our improved approach, which combines high resolution top-down and bottom-up emission data, enabling us to capture small-scale emission

https://doi.org/10.5194/egusphere-2026-3440
Preprint. Discussion started: 13 July 2026
© Author(s) 2026. CC BY 4.0 License.

areas and nonlinear responses to meteorological drivers. These are often overlooked in coarse-resolution satellite inversions or simplified statistical models.

For cropland, prior estimates range from approximately 200 to 1200 Gg N yr^{-1} (Fig. 8b), spanning statistical models (Wang et al., 2017; Gu et al., 2015; Huang et al., 2023), correction-factor approaches (Shen et al., 2022; Wu et al., 2018), data-driven methods (Ma et al., 2022), and process-based models (Huang and Li, 2014; Zhang et al., 2025). Our estimation for cropland soil NO_x emission is 623 ± 267 Gg N yr^{-1}, falling well within this range. This consistency indicates that the higher total soil NO_x emissions estimated in this study as compared to HEMCO-soil and CAMS-soil v2.4 are not due to overestimation of agricultural sources, but rather stem from improved characterization of natural ecosystems emissions, particularly from forest soils.

This conclusion is supported by comparing the emission intensities estimated in this study with those from field observations included in published literature (Tian et al., 2023; Lu et al., 2021) (Fig. 8c). Our estimated cropland emission intensity (3.8 kg N ha^{-1} yr^{-1}) exceeds the median of field observed values in the literature, which may partly reflect spatial heterogeneity in fertilization and irrigation practices that are not fully resolved at the 0.2° grid scale. For forests, our estimate (2.5 kg N ha^{-1} yr^{-1}) lies below the median of field observations, yet remains substantially higher than values in global inventories such as HEMCO-soil and CAMS-soil. This suggests that existing inventories systematically underestimate forest soil NO_x emissions in China. This underestimation is particularly pronounced in subtropical southern forests and temperate northeastern forests. The estimated grassland/shrubland emission intensity (1.9 kg N ha^{-1} yr^{-1}) is slightly higher than the few values reported in the existing literature. Given the current scarcity of published field measurements data for these ecosystems, expanding observational networks across grasslands, shrublands, and bare lands remains a priority for reducing uncertainty in future regional soil NO_x assessments.

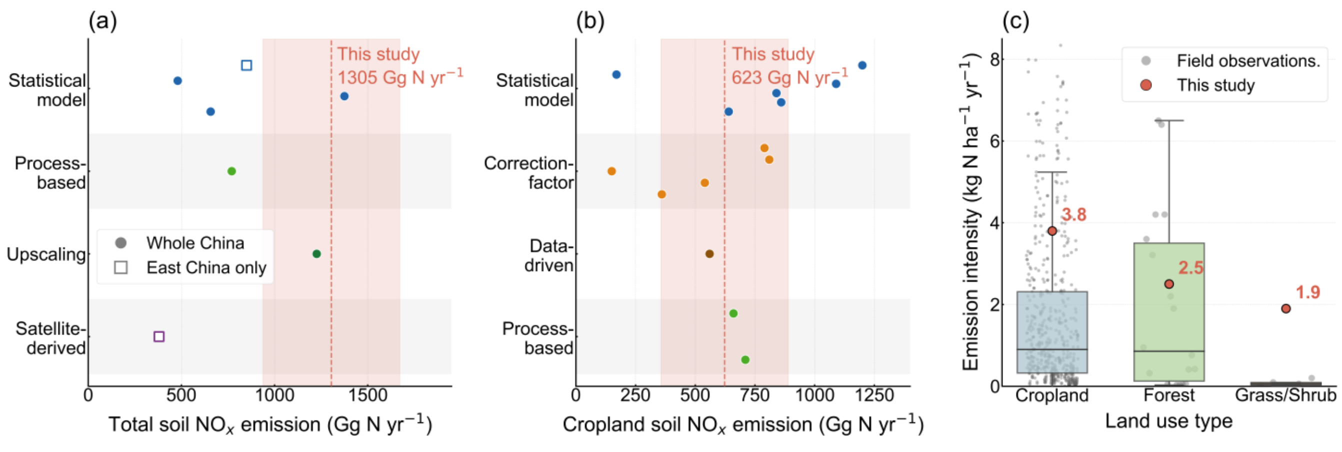

Figure 8: Comparison of (a) total soil NO_x emissions, (b) cropland soil NO_x emissions and (c) soil NO_x emission intensity between this study and published works. In (a) and (b), the red dashed line indicates the mean estimate of this study, and the shading area represents the corresponding standard deviation. In (c), the box plots denote field observations of soil emission intensity in cropland, forest and grassland/shrubland, the middle lines are the median value, the boxes top and bottom indicate the upper and lower quartiles, respectively, and the whiskers indicate the extreme non-outlier values.

https://doi.org/10.5194/egusphere-2026-3440
Preprint. Discussion started: 13 July 2026
© Author(s) 2026. CC BY 4.0 License.

5 Conclusions

In this study, we introduce a new satellite-based attribution to quantify soil NO_x emissions across eastern China at a resolution of 0.2º × 0.2º. By integrating satellite-constrained total emissions (DECSO), high-resolution anthropogenic inventory (ABaCAS-EI), land-use information and a dynamic meteorological classification method, we derive the response of land-use-specific emission intensity factors to soil temperature and moisture. The resulting parameterized temperature response functions enable grid-scale soil NO_x emission estimates to be obtained by inputting land use ratio, soil temperature, and soil moisture, facilitating the application of this approach to other regions and future climate scenarios.

Our estimate of total soil NO_x emissions from eastern China in 2019 is 1305 ± 368 Gg N. We separate these emissions across four major land use types, with cropland (623 ± 267 Gg N, ~ 48 %) and forest (486 ± 124 Gg N, ~ 37 %) as the dominant contributors. The total soil NO_x emission and cropland emissions estimates fall within the ranges reported in previous studies, supporting the reliability of our optimization approach. Compared with traditional bottom-up global emission inventories, our approach better captures the emission signals from natural ecosystems of forest in eastern China. We identify similar seasonal emissions patterns across all land use types with summer peaks, but the duration and magnitude of elevated emissions vary. Forest emissions surge in summer and remain relatively high into autumn. Cropland is the dominant source throughout the year, maintaining high emission intensity from spring to autumn. Other land use types only show some significant emissions during the summer.

We find that soil NO_x emission intensity exhibits land-use-specific responses to soil temperature and soil volumetric water content, but with a common underlying pattern: an optimum temperature for NO_x emissions exists in all land use types. Natural ecosystems generally show clear unimodal responses, with the optimum temperature at approximately 22 °C in forest, 14 °C in wet-zone grassland/shrubland, and around 32 °C in bare land. For cropland, the optimal temperature is close to or exceeds the upper limit of our observed temperature range (32 °C) due to intensive agricultural management. Therefore, the increase in temperature mainly promotes soil NO_x emissions of cropland within the observation range of this study. These land-use-specific optimum temperatures and high-temperature inhibition effects cannot be adequately captured by the monotonic functions used in conventional models.

We note that our analysis is based on monthly mean soil temperature and moisture, which cannot separate the effect of short-period soil moisture (e.g., precipitation pulses) (Huber et al., 2023) from soil temperature effects. Future research using meteorological drivers with higher temporal resolution data would help further assess the roles of soil temperature versus soil moisture in soil NO_x emissions.

In the future, the method established in this study is expected to be extended to other regions. Obtaining temperature-moisture response functions in different regions helps to construct a systematic and comprehensive framework for estimating global soil NO_x emission. This progress may further reduce current uncertainties in soil NO_x emission research, deepen our understanding of global nitrogen cycle mechanisms, and enhance our ability to predict biogenic emission trajectories under future climate scenarios.

https://doi.org/10.5194/egusphere-2026-3440
Preprint. Discussion started: 13 July 2026
© Author(s) 2026. CC BY 4.0 License.

Data availability

The DECSO total NO_x emission data used in this study are available from https://www.temis.nl/emissions/decso_nox.php, (last access: 24 September, 2025). The anthropogenic NO_x emission inventory ABaCAS-EI for 2019 is available from https://www.abacas-dss.com/abacasChinese/Software.aspx, (last access: 26 October, 2025). The CAMS-GLOB-ANT v6.2 anthropogenic emission inventory is available with a login account on the Copernicus Atmosphere Monitoring Service website at https://ads.atmosphere.copernicus.eu/datasets/cams-global-emission-inventories?tab=overview, (last access: 26 October, 2025). The ERA5-Land soil temperature and soil volumetric water content data are available on the Copernicus Climate Data Store at https://cds.climate.copernicus.eu/datasets/reanalysis-era5-land-monthly-means?tab=overview, (last access: 30 November, 2025). The CGLS-LC100m land cover product (version 3.01) for 2019 is available on the Copernicus Global Land Service website at https://land.copernicus.eu/en/products/global-dynamic-land-cover/copernicus-global-land-service-land-cover-100m-collection-3-epoch-2015-2019-globe, (last access: 18 October, 2025). The CAMS-GLOB-SOIL v2.4 and HEMCO soil NO_x emission inventories used for comparison are available from https://ads.atmosphere.copernicus.eu/datasets/cams-global-emission-inventories?tab=overview, (last access: 18 January, 2026) and https://geos-chem.s3.amazonaws.com/index.html#HEMCO/OFFLINE_SOILNOX/v2021-12/, (last access: 18 January, 2026), respectively.

Author contributions

JD and QZ designed the research. YZ and RA did the processing, visualizations, and most of the writing. JD and QZ edited the paper. XL contributed to manuscript review and editing.

Competing interests

The contact author has declared that none of the authors has any competing interests.

Disclaimer

Copernicus Publications adds a standard disclaimer: "Copernicus Publications remains neutral with regard to jurisdictional claims made in the text, published maps, institutional affiliations, or any other geographical representation in this paper. While Copernicus Publications makes every effort to include appropriate place names, the final responsibility lies with the authors. Views expressed in the text are those of the authors and do not necessarily reflect the views of the publisher."

https://doi.org/10.5194/egusphere-2026-3440
Preprint. Discussion started: 13 July 2026
© Author(s) 2026. CC BY 4.0 License.

Acknowledgements

The total satellite-derived NO_x emissions data used in this study are provided by the ESA/MOST cooperation project Dragon 6 "Air Quality Monitoring and Analysis in Populous areas in China" (AQMAP, ID95381). The anthropogenic NO_x emissions data are from ABaCAS EI and ECCAD CAMS-GLOB-ANT. The soil temperature and moisture data are provided by ECMWF ERA5-land. The land use/land cover data are supported by CGLS-LC100m. The soil NO_x emission inventories used for analysis and comparison are obtained from ECCAD CAMS-GLOB-ANT and GEOS-Chem HEMCO. This work contributes to the European Union's Horizon research and innovation programme under grant agreement no. 101183071 (GreenEO). We thank Dr. David Simpson from Norwegian Meteorological Institute for his valuable comments and stimulating discussions on this manuscript.

Financial support

This study was supported by the National Natural Science Foundation of China (NSFC; no. 42375106).

References

Buchhorn, M., Smets, B., Bertels, L., De Roo, B., Lesiv, M., Tsendbazar, N.-E., Herold, M., and Fritz, S.: Copernicus Global Land Service: Land Cover 100m (3.0.1) [dataset], https://doi.org/10.5281/zenodo.3938963, 2020a.

Buchhorn, M., Smets, B., Bertels, L., De Roo, B., Lesiv, M., Tsendbazar, N.-E., Herold, M., and Fritz, S.: Copernicus global land Service: Land cover 100m: Version 3 globe 2015-2019: Product user manual [dataset], https://doi.org/10.5281/zenodo.3938963, 2020b.

Butterbach-Bahl, K., Kahl, M., Mykhayliv, L., Werner, C., Kiese, R., and Li, C.: A European-wide inventory of soil NO emissions using the biogeochemical models DNDC/Forest-DNDC, Atmos. Environ., 43, 1392-1402, https://doi.org/10.1016/j.atmosenv.2008.02.008, 2009.

Cao, B., Gruber, S., Zheng, D., and Li, X.: The ERA5-Land soil temperature bias in permafrost regions, Cryosphere, 14, 2581-2595, https://doi.org/10.5194/tc-14-2581-2020, 2020.

Cao, P., Bilotto, F., Gonzalez Fischer, C., Mueller, N. D., Carlson, K. M., Driscoll, A. W., Gerber, J. S., Smith, P., Tubiello, F. N., West, P. C., You, L., and Herrero, M.: Spatially explicit global assessment of cropland greenhouse gas emissions circa 2020, Nat. Clim. Change, 16, 354-363, https://doi.org/10.1038/s41558-026-02558-4, 2026.

Caplin, A., Ghandehari, M., Lim, C., Glimcher, P., and Thurston, G.: Advancing environmental exposure assessment science to benefit society, Nat. Commun., 10, 1236, https://doi.org/10.1038/s41467-019-09155-4, 2019.

Dai, Z., Yu, M., Chen, H., Zhao, H., Huang, Y., Su, W., Xia, F., Chang, S. X., Brookes, P. C., Dahlgren, R. A., and Xu, J.: Elevated temperature shifts soil N cycling from microbial immobilization to enhanced mineralization, nitrification and denitrification across global terrestrial ecosystems, Global Change Biol., 26, 5267-5276, https://doi.org/10.1111/gcb.15211, 2020.

Del Grosso, S. J., Ogle, S. M., Parton, W. J., and Breidt, F. J.: Estimating uncertainty in N_2O emissions from U.S. cropland soils, Global Biogeochem. Cycles, 24, https://doi.org/10.1029/2009gb003544, 2010.

Denman, K., Brasseur, G., Chidthaisong, A., Ciais, P., Cox, P., Dickinson, R., Hauglustaine, D., Heinze, C., Holland, E., Jacob, D., Lohmann, U., Ramachandran, S., da Silva Dias, P., Wofsy, S., and Zhang, X.: Couplings between changes in the climate system and biogeochemistry, in: Climate Change 2007: The Physical Science Basis. Contribution of Working Group I to the Fourth Assessment Report of the Intergovernmental Panel on Climate Change, edited by: Solomon, S., Qin, D., Manning, M., Chen, Z., Marquis, M., Averyt, K. B., Tignor, M., and Miller, H. L., Cambridge University Press, Cambridge, UK / New York, NY, USA, 499-587, https://doi.org/10.1017/CBO9780511546013.008, 2007.

Depayras, S., Kondakova, T., Heipieper, H. J., Feuilloley, M. G. J., Orange, N., and Duclairoir-Poc, C.: The Hidden Face of Nitrogen Oxides Species: From Toxic Effects to Potential Cure?, in: Emerging Pollutants - Some Strategies for the Quality Preservation of Our Environment, edited by: Soloneski, S. and Larramendy, M. L., InTechOpen, London, 19–44, https://doi.org/10.5772/intechopen.75822, 2018.

Ding, J., van der A, R. J., Mijling, B., and Levelt, P. F.: Space-based NO_x emission estimates over remote regions improved in DECSO, Atmos. Meas. Tech., 10, 925-938, https://doi.org/10.5194/amt-10-925-2017, 2017a.

Ding, J., van der A, R. J., Mijling, B., Levelt, P. F., and Hao, N.: NO_x emission estimates during the 2014 Youth Olympic Games in Nanjing, Atmos. Chem. Phys., 15, 9399-9412, https://doi.org/10.5194/acp-15-9399-2015, 2015.

Ding, J., van der A, R. J., Mijling, B., Jalkanen, J. P., Johansson, L., and Levelt, P. F.: Maritime NOx Emissions Over Chinese Seas Derived From Satellite Observations, Geophys. Res. Lett., 45, 2031-2037, https://doi.org/10.1002/2017gl076788, 2018.

Ding, J., van der A, R. J., Eskes, H. J., Mijling, B., Stavrakou, T., van Geffen, J. H. G. M., and Veefkind, J. P.: NOx Emissions Reduction and Rebound in China Due to the COVID-19 Crisis, Geophys. Res. Lett., 46, https://doi.org/10.1029/2020gl089912, 2020.

Ding, J., Miyazaki, K., van der A, R. J., Mijling, B., Kurokawa, J.-i., Cho, S., Janssens-Maenhout, G., Zhang, Q., Liu, F., and Levelt, P. F.: Intercomparison of NO_x emission inventories over East Asia, Atmos. Chem. Phys., 17, 10125-10141, https://doi.org/10.5194/acp-17-10125-2017, 2017b.

Firestone, M. K. and Davidson, E. A.: Microbiological basis of NO and N_2O production and consumption in soil, in: Exchange of Trace Gases between Terrestrial Ecosystems and the Atmosphere, edited by: Andreae, M. O., and Schimel, D. S., John Wiley & Sons, 7-21, 1989.

Fowler, D., Coyle, M., Skiba, U., Sutton, M. A., Cape, J. N., Reis, S., Sheppard, L. J., Jenkins, A., Grizzetti, B., Galloway, J. N., Vitousek, P., Leach, A., Bouwman, A. F., Butterbach-Bahl, K., Dentener, F., Stevenson, D., Amann, M., and Voss, M.: The global nitrogen cycle in the twenty-first century, Philos. Trans. R. Soc. B, 368, 20130164, https://doi.org/10.1098/rstb.2013.0164, 2013.

© Author(s) 2026. CC BY 4.0 License.

Frey, H. C., Bharvirkar, R., Thompson, T., and Bromberg, S.: Quantification of Variability and Uncertainty in Emission Factors and Inventories, Proceedings of the 91st Annual Meeting of the Air & Waste Management Association, San Diego, CA, USA1998.

Gu, B., Ju, X., Chang, J., Ge, Y., and Vitousek, P. M.: Integrated reactive nitrogen budgets and future trends in China, Proc. Natl. Acad. Sci., 112, 8792-8797, https://doi.org/10.1073/pnas.1510211112, 2015.

Guo, L., Chen, J., Luo, D., Liu, S., Lee, H. J., Motallebi, N., Fong, A., Deng, J., Rasool, Q. Z., Avise, J. C., Kuwayama, T., Croes, B. E., and FitzGibbon, M.: Assessment of Nitrogen Oxide Emissions and San Joaquin Valley $PM_{2.5}$ Impacts From Soils in California, J. Geophys. Res.: Atmos., 125, https://doi.org/10.1029/2020jd033304, 2020.

Holland, E. A., Dentener, Frank J., Braswell, Bobby H., and Sulzman, James M.: Contemporary and pre-industrial global reactive nitrogen budgets, Biogeochemistry, 46, 7-43, 1999.

Huang, K., Wu, D., Liu, D., Duan, Y., Dorsch, P., Butterbach-Bahl, K., Fang, X., Liu, Y., Wang, C., Yu, H., Qu, L., Xu, J., Gurmesa, G. A., Kang, R., Peng, S., Hobbie, E. A., Ju, X., Hu, S., Phillips, O. L., Gundersen, P., Zhu, W., Homyak, P. M., and Fang, Y.: Climate warming reduces soil gaseous nitrogen losses in a temperate forest, Proc. Natl. Acad. Sci., 122, e2513401122, https://doi.org/10.1073/pnas.2513401122, 2025.

Huang, L., Fang, J., Liao, J., Yarwood, G., Chen, H., Wang, Y., and Li, L.: Insights into soil NO emissions and the contribution to surface ozone formation in China, Atmos. Chem. Phys., 23, 14919-14932, https://doi.org/10.5194/acp-23-14919-2023, 2023.

Huang, Y. and Li, D.: Soil nitric oxide emissions from terrestrial ecosystems in China: a synthesis of modeling and measurements, Sci. Rep., 4, https://doi.org/10.1038/srep07406, 2014.

Huber, D. E., Steiner, A. L., and Kort, E. A.: Sensitivity of Modeled Soil NOx Emissions to Soil Moisture, J. Geophys. Res.: Atmos., 128, https://doi.org/10.1029/2022jd037611, 2023.

Hudman, R. C., Moore, N. E., Mebust, A. K., Martin, R. V., Russell, A. R., Valin, L. C., and Cohen, R. C.: Steps towards a mechanistic model of global soil nitric oxide emissions: implementation and space based-constraints, Atmos. Chem. Phys., 12, 7779-7795, https://doi.org/10.5194/acp-12-7779-2012, 2012.

Jaegle, L., Steinberger, L., Martin, R. V., and Chance, K.: Global partitioning of NO_x sources using satellite observations: relative roles of fossil fuel combustion, biomass burning and soil emissions, Faraday Discuss., 130, 407-423; discussion 491-517, 519-424, https://doi.org/10.1039/b502128f, 2005.

Keller, C. A., Long, M. S., Yantosca, R. M., Da Silva, A. M., Pawson, S., and Jacob, D. J.: HEMCO v1.0: a versatile, ESMF-compliant component for calculating emissions in atmospheric models, Geosci. Model Dev., 7, 1409-1417, https://doi.org/10.5194/gmd-7-1409-2014, 2014.

Kesik, M., Ambus, P., Baritz, R., Bruggemann, N., Butterbach-Bahl, K., Damm, M., Duyzer, J., Horvath, L., Kiese, R., Kitzler, B., Leip, A., Li, C., Pihlatie, M., Pilegaard, K., Seufert, G., Simpson, D., Skiba, U., Smiatek, G., Vesala, T., and Zechmeister-Boltenstern, S.: Inventories of N_2O and NO emissions from European forest soils, Biogeosciences, 2, 353-375, 2005.

Kottek, M., Grieser, J., Beck, C., Rudolf, B., and Rubel, F.: World Map of the Köppen-Geiger climate classification updated, Meteorol. Z., 15, 259-263, https://doi.org/10.1127/0941-2948/2006/0130, 2006.

https://doi.org/10.5194/egusphere-2026-3440
Preprint. Discussion started: 13 July 2026
© Author(s) 2026. CC BY 4.0 License.

Li, C., van Donkelaar, A., Hammer, M. S., McDuffie, E. E., Burnett, R. T., Spadaro, J. V., Chatterjee, D., Cohen, A. J., Apte, J. S., Southerland, V. A., Anenberg, S. C., Brauer, M., and Martin, R. V.: Reversal of trends in global fine particulate matter air pollution, Nat. Commun., 14, 5349, https://doi.org/10.1038/s41467-023-41086-z, 2023a.

Li, H., Zheng, B., Lei, Y., Hauglustaine, D., Chen, C., Lin, X., Zhang, Y., Zhang, Q., and He, K.: Trends and drivers of anthropogenic NO_x emissions in China since 2020, Environ. Sci. Ecotechnol., 21, 100425, https://doi.org/10.1016/j.ese.2024.100425, 2024a.

Li, M., Kurokawa, J., Zhang, Q., Woo, J.-H., Morikawa, T., Chatani, S., Lu, Z., Song, Y., Geng, G., Hu, H., Kim, J., Cooper, O. R., and McDonald, B. C.: MIXv2: a long-term mosaic emission inventory for Asia (2010–2017), Atmos. Chem. Phys., 24, 3925-3952, https://doi.org/10.5194/acp-24-3925-2024, 2024b.

Li, S., Wang, S., Wu, Q., Zhang, Y., Ouyang, D., Zheng, H., Han, L., Qiu, X., Wen, Y., Liu, M., Jiang, Y., Yin, D., Liu, K., Zhao, B., Zhang, S., Wu, Y., and Hao, J.: Emission trends of air pollutants and CO_2 in China from 2005 to 2021, Earth Syst. Sci. Data, 15, 2279-2294, https://doi.org/10.5194/essd-15-2279-2023, 2023b.

Lin, J. T.: Satellite constraint for emissions of nitrogen oxides from anthropogenic, lightning and soil sources over East China on a high-resolution grid, Atmos. Chem. Phys., 12, 2881-2898, https://doi.org/10.5194/acp-12-2881-2012, 2012.

Lin, X., van der A, R., de Laat, J., Huijnen, V., Mijling, B., Ding, J., Eskes, H., Douros, J., Liu, M., Zhang, X., and Liu, Z.: European Soil NO_x Emissions Derived From Satellite NO_2 Observations, J. Geophys. Res.: Atmos., 129, https://doi.org/10.1029/2024jd041492, 2024.

Logan, J. A.: Nitrogen oxides in the troposphere: Global and regional budgets, J. Geophys. Res.: Oceans, 88, 10785-10807, https://doi.org/10.1029/JC088iC15p10785, 1983.

Lu, X., Ye, X., Zhou, M., Zhao, Y., Weng, H., Kong, H., Li, K., Gao, M., Zheng, B., Lin, J., Zhou, F., Zhang, Q., Wu, D., Zhang, L., and Zhang, Y.: The underappreciated role of agricultural soil nitrogen oxide emissions in ozone pollution regulation in North China, Nat. Commun., 12, 5021, https://doi.org/10.1038/s41467-021-25147-9, 2021.

Ma, R., Yu, K., Xiao, S., Liu, S., Ciais, P., and Zou, J.: Data-driven estimates of fertilizer-induced soil NH_3 , NO and N_2O emissions from croplands in China and their climate change impacts, Global Change Biol., 28, 1008-1022, https://doi.org/10.1111/gcb.15975, 2022.

Menut, L., Bessagnet, B., Briant, R., Cholakian, A., Couvidat, F., Mailler, S., Pennel, R., Siour, G., Tuccella, P., Turquety, S., and Valari, M.: The CHIMERE v2020r1 online chemistry-transport model, Geosci. Model Dev., 14, 6781-6811, https://doi.org/10.5194/gmd-14-6781-2021, 2021.

Metropolis, N. and Ulam, S.: The Monte Carlo Method, J. Am. Stat. Assoc., 44, 335-341, 1949.

Mijling, B. and van der A, R. J.: Using daily satellite observations to estimate emissions of short-lived air pollutants on a mesoscopic scale, J. Geophys. Res.: Atmos., 117, https://doi.org/10.1029/2012jd017817, 2012.

Molina-Herrera, S., Haas, E., Grote, R., Kiese, R., Klatt, S., Kraus, D., Kampffmeyer, T., Friedrich, R., Andreae, H., Loubet, B., Ammann, C., Horváth, L., Larsen, K., Gruening, C., Frumau, A., and Butterbach-Bahl, K.: Importance of soil NO emissions for the total atmospheric NO_x budget of Saxony, Germany, Atmos. Environ., 152, 61-76, https://doi.org/10.1016/j.atmosenv.2016.12.022, 2017.

Morichetti, M., Madronich, S., Passerini, G., Rizza, U., Mancinelli, E., Virgili, S., and Barth, M.: Comparison and evaluation of updates to WRF-Chem (v3.9) biogenic emissions using MEGAN, Geosci. Model Dev., 15, 6311-6339, https://doi.org/10.5194/gmd-15-6311-2022, 2022.

Muñoz-Sabater, J., Dutra, E., Agustí-Panareda, A., Albergel, C., Arduini, G., Balsamo, G., Boussetta, S., Choulga, M., Harrigan, S., Hersbach, H., Martens, B., Miralles, D. G., Piles, M., Rodríguez-Fernández, N. J., Zsoter, E., Buontempo, C., and Thépaut, J.-N.: ERA5-Land: a state-of-the-art global reanalysis dataset for land applications, Earth Syst. Sci. Data, 13, 4349-4383, https://doi.org/10.5194/essd-13-4349-2021, 2021.

Pietikainen, J., Pettersson, M., and Baath, E.: Comparison of temperature effects on soil respiration and bacterial and fungal growth rates, FEMS Microbiol. Ecol., 52, 49-58, https://doi.org/10.1016/j.femsec.2004.10.002, 2005.

Pilegaard, K.: Processes regulating nitric oxide emissions from soils, Philos. Trans. R. Soc. B, 368, 20130126, https://doi.org/10.1098/rstb.2013.0126, 2013.

Rafaj, P., Amann, M., Siri, J., and Wuester, H.: Changes in European greenhouse gas and air pollutant emissions 1960–2010: decomposition of determining factors, Clim. Change, 124, 477-504, https://doi.org/10.1007/s10584-013-0826-0, 2013.

Rijsdijk, P., Eskes, H., Dingemans, A., Boersma, K. F., Sekiya, T., Miyazaki, K., and Houweling, S.: Quantifying uncertainties in satellite NO_2 superobservations for data assimilation and model evaluation, Geosci. Model Dev., 18, 483-509, https://doi.org/10.5194/gmd-18-483-2025, 2025.

Schumann, U. and Huntrieser, H.: The global lightning-induced nitrogen oxides source, Atmos. Chem. Phys., 7, 3823-3907, https://doi.org/10.5194/acp-7-3823-2007, 2007.

Sha, T., Ma, X., Zhang, H., Janechek, N., Wang, Y., Wang, Y., Castro Garcia, L., Jenerette, G. D., and Wang, J.: Impacts of Soil NO_x Emission on O_3 Air Quality in Rural California, Environ. Sci. Technol., 55, 7113-7122, https://doi.org/10.1021/acs.est.0c06834, 2021.

Shen, Y., Xiao, Z., Wang, Y., Yao, L., and Xiao, W.: Multisource Remote Sensing Based Estimation of Soil NO_x Emissions From Fertilized Cropland at High-Resolution: Spatio-Temporal Patterns and Impacts, J. Geophys. Res.: Atmos., 127, https://doi.org/10.1029/2022jd036741, 2022.

Simpson, D. and Darras, S.: Global soil NO emissions for Atmospheric Chemical Transport Modelling: CAMS-GLOB-SOIL v2.2, Earth Syst. Sci. Data Discuss., https://doi.org/10.5194/essd-2021-221, 2021.

Simpson, D., Benedictow, A., and Darras, S.: The CAMS soil emissions: CAMS-GLOB-SOIL, in: Documentation of CAMS emission inventory products, edited by: Denier van der Gon, H., Gauss, M., and Granier, C., Copernicus Atmosphere Monitoring Service, 68-80, https://doi.org/10.24380/uag-0svt, 2025.

Soulie, A., Granier, C., Darras, S., Zilbermann, N., Doumbia, T., Guevara, M., Jalkanen, J.-P., Keita, S., Liousse, C., Crippa, M., Guizzardi, D., Hoesly, R., and Smith, S. J.: Global anthropogenic emissions (CAMS-GLOB-ANT) for the Copernicus

Atmosphere Monitoring Service simulations of air quality forecasts and reanalyses, Earth Syst. Sci. Data, 16, 2261-2279, https://doi.org/10.5194/essd-16-2261-2024, 2024.

Steinkamp, J. and Lawrence, M. G.: Influence of modelled soil biogenic NO emissions on related trace gases and the atmospheric oxidizing efficiency, Atmos. Chem. Phys., 9, 2662-2677, 2009.

Steinkamp, J. and Lawrence, M. G.: Improvement and evaluation of simulated global biogenic soil NO emissions in an AC-GCM, Atmos. Chem. Phys., 11, 6063-6082, https://doi.org/10.5194/acp-11-6063-2011, 2011.

Sun, S., Sun, L., Liu, G., Zou, C., Wang, Y., Wu, L., and Mao, H.: Developing a vehicle emission inventory with high temporal-spatial resolution in Tianjin, China, Sci. Total Environ., 776, https://doi.org/10.1016/j.scitotenv.2021.145873, 2021.

Tan, X., Luo, S., Li, H., Li, Z., and Dong, Q.: A soil temperature dataset based on random forest in the Three River Source Region, Sci. Data, 12, 882, https://doi.org/10.1038/s41597-025-04910-3, 2025.

Tian, X., Yin, Y., He, K., Qiu, R., Cong, J., Wang, Z., Yu, H., Chen, Z., Chu, Y., Ying, H., and Cui, Z.: Data-driven estimation of nitric oxide emissions from global soils based on dominant vegetation covers, Global Change Biol., 29, 5955-5967, https://doi.org/10.1111/gcb.16864, 2023.

Tie, X., Li, G., Ying, Z., Guenther, A., and Madronich, S.: Biogenic emissions of isoprenoids and NO in China and comparison to anthropogenic emissions, Sci. Total Environ., 371, 238-251, https://doi.org/10.1016/j.scitotenv.2006.06.025, 2006.

van der A, R. J., Ding, J., and Eskes, H.: Monitoring European anthropogenic NO_x emissions from space, Atmos. Chem. Phys., 24, 7523-7534, https://doi.org/10.5194/acp-24-7523-2024, 2024.

van der A, R. J., Mijling, B., Ding, J., Koukouli, M. E., Liu, F., Li, Q., Mao, H., and Theys, N.: Cleaning up the air: effectiveness of air quality policy for SO_2 and NO_x emissions in China, Atmos. Chem. Phys., 17, 1775-1789, https://doi.org/10.5194/acp-17-1775-2017, 2017.

Veefkind, J. P., Aben, I., McMullan, K., Förster, H., de Vries, J., Otter, G., Claas, J., Eskes, H. J., de Haan, J. F., Kleipool, Q., van Weele, M., Hasekamp, O., Hoogeveen, R., Landgraf, J., Snel, R., Tol, P., Ingmann, P., Voors, R., Kruizinga, B., Vink, R., Visser, H., and Levelt, P. F.: TROPOMI on the ESA Sentinel-5 Precursor: A GMES mission for global observations of the atmospheric composition for climate, air quality and ozone layer applications, Remote Sens. Environ., 120, 70-83, https://doi.org/10.1016/j.rse.2011.09.027, 2012.

Verchot, L. V., Davidson, E. A., Cattânio, H., Ackerman, I. L., Erickson, H. E., and Keller, M.: Land use change and biogeochemical controls of nitrogen oxide emissions from soils in eastern Amazonia, Global Biogeochem. Cycles, 13, 31-46, https://doi.org/10.1029/1998GB900019, 1999.

Vinken, G. C. M., Boersma, K. F., Maasakkers, J. D., Adon, M., and Martin, R. V.: Worldwide biogenic soil NO_x emissions inferred from OMI NO_2 observations, Atmos. Chem. Phys., 14, 10363-10381, https://doi.org/10.5194/acp-14-10363-2014, 2014.

Wang, M., Kroeze, C., Strokal, M., and Ma, L.: Reactive nitrogen losses from China's food system for the shared socioeconomic pathways (SSPs), Sci. Total Environ., 605-606, 884-893, https://doi.org/10.1016/j.scitotenv.2017.06.235, 2017.

https://doi.org/10.5194/egusphere-2026-3440
Preprint. Discussion started: 13 July 2026
© Author(s) 2026. CC BY 4.0 License.

Wang, R., Bei, N., Wu, J., Li, X., Liu, S., Yu, J., Jiang, Q., Tie, X., and Li, G.: Cropland nitrogen dioxide emissions and effects on the ozone pollution in the North China plain, Environ. Pollut., 294, 118617, https://doi.org/10.1016/j.envpol.2021.118617, 2022.

Wang, Y., Ge, C., Castro Garcia, L., Jenerette, G. D., Oikawa, P. Y., and Wang, J.: Improved modelling of soil NO_x emissions in a high temperature agricultural region: role of background emissions on NO_2 trend over the US, Environ. Res. Lett., 16, https://doi.org/10.1088/1748-9326/ac16a3, 2021.

Wang, Y., McElroy, M. B., Martin, R. V., Streets, D. G., Zhang, Q., and Fu, T. M.: Seasonal variability of NO_x emissions over east China constrained by satellite observations: Implications for combustion and microbial sources, J. Geophys. Res.: Atmos., 112, https://doi.org/10.1029/2006jd007538, 2007.

Wang, Y., Wang, Y., Li, Q., Tan, Y., Li, M., Zhang, Y., He, C., and Wang, T.: Soil Emissions of Reactive Oxidized Nitrogen Reduce the Effectiveness of Anthropogenic Source Control in China, Environ. Sci. Technol., 58, 21015-21024, https://doi.org/10.1021/acs.est.4c08526, 2024.

Wei, W., Wang, S., and Hao, J.: Uncertainty Analysis of Emission Inventory for Volatile Organic Compounds from Anthropogenic Sources in China, Environmental Science, 32, 305-312, https://doi.org/10.13227/j.hjkx.2011.02.021, 2011.

Weng, H., Lin, J., Martin, R., Millet, D. B., Jaegle, L., Ridley, D., Keller, C., Li, C., Du, M., and Meng, J.: Global high-resolution emissions of soil NO_x, sea salt aerosols, and biogenic volatile organic compounds, Sci. Data, 7, 148, https://doi.org/10.1038/s41597-020-0488-5, 2020.

Winiwarter, W. and Muik, B.: Statistical dependence in input data of national greenhouse gas inventories: effects on the overall inventory uncertainty, Clim. Change, 103, 19-36, https://doi.org/10.1007/s10584-010-9921-7, 2010.

Wu, H., Wang, S., Gao, L., Zhang, L., Yuan, Z., Fan, T., Wei, K., and Huang, L.: Nutrient-derived environmental impacts in Chinese agriculture during 1978-2015, J. Environ. Manage., 217, 762-774, https://doi.org/10.1016/j.jenvman.2018.04.002, 2018.

Yan, X., Ohara, T., and Akimoto, H.: Statistical modeling of global soil NO_x emissions, Global Biogeochem. Cycles, 19, https://doi.org/10.1029/2004gb002276, 2005.

Yang, S., Li, R., Wu, T., Hu, G., Xiao, Y., Du, Y., Zhu, X., Ni, J., Ma, J., Zhang, Y., Shi, J., and Qiao, Y.: Evaluation of reanalysis soil temperature and soil moisture products in permafrost regions on the Qinghai-Tibetan Plateau, Geoderma, 377, https://doi.org/10.1016/j.geoderma.2020.114583, 2020.

Yienger, J. J. and Levy, H., II: Empirical model of global soil-biogenic NO_x emission, J. Geophys. Res., 100, 11447-11464, 1995.

Zhang, M., Zhang, X., Gao, C., Zhao, H., Zhang, S., Xie, S., Ran, L., and Xiu, A.: Reactive nitrogen emissions from cropland and their dominant driving factors in China, Sci. Total Environ., 968, 178919, https://doi.org/10.1016/j.scitotenv.2025.178919, 2025.

Zhang, R., Tie, X., and Bond, D. W.: Impacts of anthropogenic and natural NO_x sources over the U.S. on tropospheric chemistry, Proc. Natl. Acad. Sci., 100, 1505-1509, https://doi.org/10.1073/pnas.252763799, 2003.

https://doi.org/10.5194/egusphere-2026-3440
Preprint. Discussion started: 13 July 2026
© Author(s) 2026. CC BY 4.0 License.

Zhang, T., Yue, X., Unger, N., Feng, Z., Zheng, B., Li, T., Lei, Y., Zhou, H., Dong, X., Liu, Y., Zhu, J., and Yang, X.: Modeling the joint impacts of ozone and aerosols on crop yields in China: An air pollution policy scenario analysis, Atmos. Environ., 247, https://doi.org/10.1016/j.atmosenv.2021.118216, 2021.

Zhang, X., van der A, R., Ding, J., Zhang, X., and Yin, Y.: Significant contribution of inland ships to the total NO_x emissions along the Yangtze River, Atmos. Chem. Phys., 23, 5587-5604, https://doi.org/10.5194/acp-23-5587-2023, 2023.

Zhao, B., Wang, S. X., Liu, H., Xu, J. Y., Fu, K., Klimont, Z., Hao, J. M., He, K. B., Cofala, J., and Amann, M.: NO_x emissions in China: historical trends and future perspectives, Atmos. Chem. Phys., 13, 9869-9897, https://doi.org/10.5194/acp-13-9869-2013, 2013.

Zhao, B., Zheng, H., Wang, S., Smith, K. R., Lu, X., Aunan, K., Gu, Y., Wang, Y., Ding, D., Xing, J., Fu, X., Yang, X., Liou, K. N., and Hao, J.: Change in household fuels dominates the decrease in $PM_{2.5}$ exposure and premature mortality in China in 2005-2015, Proc. Natl. Acad. Sci., 115, 12401-12406, https://doi.org/10.1073/pnas.1812955115, 2018.

Zhao, C. and Wang, Y.: Assimilated inversion of NO_x emissions over east Asia using OMI NO_2 column measurements, Geophys. Res. Lett., 36, https://doi.org/10.1029/2008gl037123, 2009.

Zheng, H., Zhao, B., Wang, S., Wang, T., Ding, D., Chang, X., Liu, K., Xing, J., Dong, Z., Aunan, K., Liu, T., Wu, X., Zhang, S., and Wu, Y.: Transition in source contributions of $PM_{2.5}$ exposure and associated premature mortality in China during 2005–2015, Environ. Int., 132, 105111, https://doi.org/10.1016/j.envint.2019.105111, 2019.

Zheng, Y., Coxon, G., Woods, R., Power, D., Rico-Ramirez, M. A., McJannet, D., Rosolem, R., Li, J., and Feng, P.: Evaluation of reanalysis soil moisture products using cosmic ray neutron sensor observations across the globe, Hydrol. Earth Syst. Sci., 28, 1999-2022, https://doi.org/10.5194/hess-28-1999-2024, 2024.

Zhou, Z., Zheng, X., Xie, B., Liu, C., Song, T., Han, S., and Zhu, J.: Nitric oxide emissions from rice-wheat rotation fields in eastern China: effect of fertilization, soil water content, and crop residue, Plant Soil, 336, 87-98, https://doi.org/10.1007/s11104-010-0450-y, 2010.